Article

A First Assessment of the 2018 European Drought Impact on Ecosystem Evapotranspiration

Kazi Rifat Ahmed [1],*, Eugénie Paul-Limoges [1] , Uwe Rascher [2] and Alexander Damm [1,3]

[1] Department of Geography, University of Zurich, Winterthurerstrasse 190, 8057 Zurich, Switzerland; eugenie.paul-limoges@geo.uzh.ch (E.P.-L.); alexander.damm@geo.uzh.ch (A.D.)
[2] Plant Science (IBG-2), Institute of Bio- and Geosciences, Forschungszentrum Jülich, Leo-Brandt-Str, 52425 Jülich, Germany; u.rascher@fz-juelich.de
[3] Swiss Federal Institute of Aquatic Science and Technology, Surface Waters — Research and Management, Überlandstrasse 133, 8600 Dübendorf, Switzerland
* Correspondence: rifat.ahmed@geo.uzh.ch

Abstract: The combined heatwave and drought in 2018 notably affected the state and functioning of European ecosystems. The severity and distribution of this extreme event across ecosystem types and its possible implication on ecosystem water fluxes are still poorly understood. This study estimates spatio-temporal changes in evapotranspiration (ET) during the 2018 drought and heatwave and assesses how these changes are distributed in European ecosystems along climatic gradients. We used the ET eight-day composite product from the MODerate Resolution Imaging Spectroradiometer (MODIS) together with meteorological data from the European Centre for Medium-Range Weather Forecasts (ECMWF ERA5). Our results indicate that ecosystem ET was strongly reduced (up to -50% compared to a 10-year reference period) in areas with extreme anomalies in surface air temperature (T_{sa}) and precipitation (P) in central, northern, eastern, and western Europe. Northern and Eastern Europe had prolonged anomalies of up to seven months with extreme intensities (relative and absolute) of T_{sa}, P, and ET. Particularly, agricultural areas, mixed natural vegetation, and non-irrigated agricultural areas were the most affected by the increased temperatures in northern Europe. Our results show contrasting drought impacts on ecosystem ET between the North and South of Europe as well as on ecosystem types.

Keywords: European drought; European heat-wave; European ecosystems; evapotranspiration anomalies; MODIS evapotranspiration; precipitation; temperature

1. Introduction

Extreme climate events can substantially alter the state and integrity of ecosystems. Particularly the increased frequency and duration of such events (i.e., droughts and heat-waves) substantially impact energy and water fluxes in ecosystems [1,2] and cause various feedbacks between the atmosphere and the biosphere [3,4]. A recent example is the combined European drought and heatwave of 2018 that severely affected European ecosystems, caused severe damages and substantially altered the functioning of these ecosystems [5,6]. This extreme event has been characterized as exceptionally warm, especially around its epicenter in northern and central Europe [7]. Detailed knowledge of underlying mechanisms and feedbacks is pivotal to understand causes of resulting ecosystem alterations and to assess future trajectories of ecosystems in the context of ongoing environmental change.

Evapotranspiration (ET) is defined as one of the main environmental variables for determining the response of the terrestrial biosphere to extreme climate events [3,8]. Recent studies reported a decline in ET in the past decades and observed some substantial feedback with increasing temperature and drought [9,10]. These complex interplays depend on regional climatic variability and ecosystem conditions [10,11]. Other studies indicated changing ET pattern due to climate change and related drought events [1,12–15], having

substantial implications for food security and water resource management worldwide [16]. As an example, the 2003 European drought reduced gross primary production (GPP) by approximately 20%, representing a direct plant physiological response to drought stress [17]. This study also showed that during the 2003 drought, especially soil drought together with a high vapor pressure deficit (VPD) determined stomatal closure and reduced GPP and ET [2]. Another study indicated that under extreme soil drought, both ET and GPP decreased with increasing VPD, while ET and GPP were linked non-linearly and changed simultaneously [18]. Consequently, assessing spatio-temporal patterns of drought caused ET dynamics is essential to advance in-depth understanding on the impact of extreme events on ecosystem ET, and thus the state and functioning of ecosystems.

The underlying complexity of ET and many interwoven relations between ET and other ecosystem processes and properties, however, challenges the assessment of drought-induced ET changes. A drought is defined by the change of multiple variables, e.g., surface air temperature (T_{sa}) [19–21], precipitation (P) [19,20,22,23], soil moisture [24], water storage [25], and surface and subsurface runoff [25]. These variables also ultimately influence ET at different spatio-temporal scales [21,26–28]. This explains why changes in ET have been used for the identification of droughts [24]. Since the determinants for drought and ET are closely linked, care must be taken to assess the impact of drought on ET [24,25]. Previous studies highlighted P as the main driver for droughts [29], while the combination of P and T_{sa} are suggested as the main drivers for events comprising a drought and a heatwave. Feedbacks between ET and local meteorology can also intensify droughts [30]. In addition to water availability, energy and atmospheric constraints, ET additionally depends on several plant physiological responses and other surface properties. Therefore, drought caused ET changes are complex phenomenon that largely depend on the underlying ecosystem and vegetation type [31,32].

The aim of this study is to quantify the impact of the combined drought and heatwave in 2018 on ecosystem ET, and to assess how these changes are distributed in different ecosystem types along climatic gradients in Europe. We used established globally available ET estimates (i.e., the MODerate Resolution Imaging Spectroradiometer (MODIS) global eight-day composite), and T_{sa} and P meteorological fields (i.e., European Centre for Medium-Range Weather Forecasts, ECMWF ERA5 data). We combined these data and a mechanistic data modeling approach (a) to quantify characteristics of the combined heatwave and drought in Europe in 2018, (b) to assess spatio-temporal ET anomalies during the extreme year 2018 compared to a reference period from 2007 to 2017, (c) to estimate the impact of the meteorological drivers on ET anomalies, and (d) to quantify drought caused ecosystem specific ET anomalies in selected regions.

2. Materials and Methods

2.1. Study Area

The study area spans Europe (Figure 1) and covers different ecosystems, including croplands, mixed agricultural lands, grasslands, wetlands, and forests. The study area covers a range of environmental and climatic conditions, from higher Alpine to lower sea coast, and includes temperate, tundra, boreal, sub-tropical, and Mediterranean climates. These different climates and vegetation ecosystems facilitate a throughout assessment of ET dynamics induced by the 2018 extreme event.
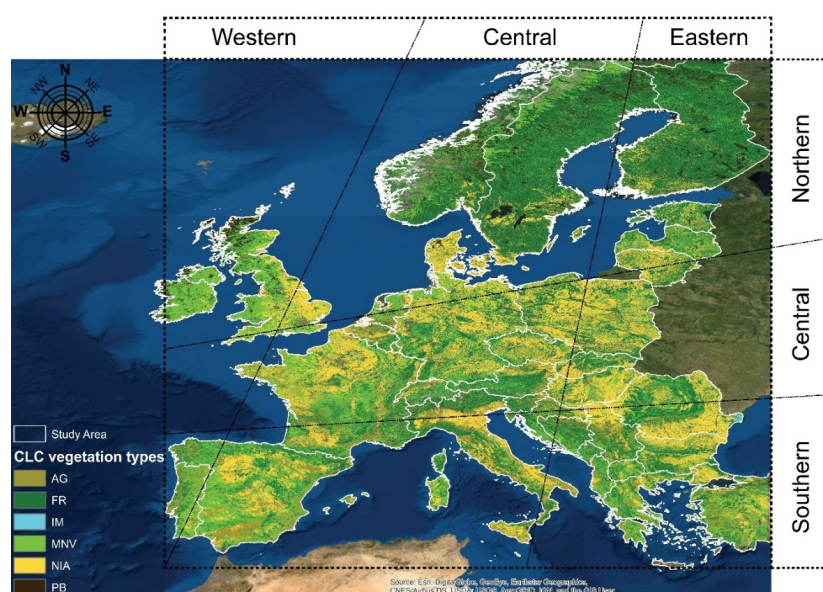
Figure 1. Map of the study area with six different vegetation types—agriculture (AG), forest (FR), inland marsh (IM), mixed natural vegetation (MNV), non-irrigated arable land (NIA), and peat bog vegetation (PB). Vegetation classes are derived from the CORINE Land Cover data set (CLC 2018), Land Monitoring Service, Copernicus Program (https://land.copernicus.eu/pan-european/corine-land-cover/clc2018). The white border indicates the study area. Background image source: Esri, DigitalGlobe, GeoEye, Earthstar Geographics, CNES/Airbus DS, USDA, USGS, AeroGRID, IGN, and the GIS User Community.

2.2. Data

2.2.1. Evapotranspiration and Meteorological Data

We used the MODIS global 8-day composites of total daily potential ET (MOD16A2 version 6) with 500 m pixel resolution [33,34]. The used MODIS-ET product version is based on the algorithm described in [34] and relies on the Penman–Monteith modeling framework [35,36] with advanced calculations of daytime and nighttime ET, vegetation cover fraction, stomatal conductance, aerodynamic conductance, boundary layer resistance, soil heat flux, dry and wet surface fraction, and saturated and wet soil surface [34]. The performance of the algorithm has been previously validated and tested with data from AmeriFlux eddy covariance towers [34].

Additionally, we used two meteorological variables, including total P (in m), and T_{sa} measured at 2 m above ground (in K). P and T_{sa} data were collected from ECMWF ERA5 hourly data on single levels with $0.25° \times 0.25°$ spatial resolution (C3S ERA5: https://cds.climate.copernicus.eu/cdsapp#!/dataset/reanalysis-era5-single-levels?tab=overview).

2.2.2. Land Cover Data

We used the CORINE Land Cover data set (CLC 2018) of the Land Monitoring Service by Copernicus Programme (https://land.copernicus.eu/pan-european/corine-land-cover/clc2018) to enable an assessment of ET changes in specific vegetation ecosystems. The spatial resolution of the CLC 2018 data is 10 m with a thematic accuracy of larger than 85%. The CLC map was obtained as a shapefile from the European Copernicus program (https://land.copernicus.eu/pan-european/corine-land-cover) and converted into a raster file format to eventually mask different vegetation ecosystems in the study area.

2.3. Data Processing and Analysis

The retrieval of co-registered monthly averages of MODIS ET and meteorological data for 2018 and a 10-year reference period was done in the Google Earth Engine (GEE) application programming interface (API). The GEE API was used under a free open

source license and offered a cloud-based data analytics infrastructure. A detailed description of GEE analytical infrastructure can be found in [37]. The GEE API facilitates the efficient processing of big satellite data and offers extensive processing capabilities and computational robustness in terms of large volume data analysis. All other analytical steps and the visualization of results was done using Python (version 3.7), particularly ipython [38]. The complete processing code is based on different Python libraries and APIs, i.e., scipy [39], numpy [40], pandas [41], matplotlib [42], and rasterio api (https://rasterio.readthedocs.io/en/latest/intro.html).

2.4. Calculation of Anomalies Per Month

We calculated monthly ET, P, or T_{sa} anomalies (ΔV_m, V represents ET, P, or T_{sa}, respectively) in 2018 as the normalized difference of monthly data in the drought year 2018 ($V_{2018,m}$) and the reference period spanning 2007–2017 ($V_{mean,m}$):

$$\Delta V_m = \frac{V_{2018,m} - V_{mean,m}}{V_{mean,m}} \times 100\% \tag{1}$$

2.5. Method for Identifying Onset, Length, and Intensity of the Drought

Monthly anomaly maps between April and October are further used to quantify ET responses and drought characteristics in terms of onset, length, and intensity. The onset was defined as the first month with negative (for ET and P) and positive (for T_{sa}) anomalies (i.e., the first month of the anomaly time series corresponds to April, the last to October). The length represents the number of months with negative anomalies for ET and P, and positive anomalies for T_{sa}. We calculated the seasonal cumulated anomaly as absolute intensity (I_a) and relative intensity (I_r) for ET, P, and T_{sa}. I_a represents the seasonal sum of differences between monthly anomalies in 2018 ($\Delta_{2018,m}$) and the reference period (2007 to 2017) ($\Delta_{mean,m}$) in physical units as

$$I_a = \sum_{m=1}^{7} [\Delta_{2018,m} - \Delta_{mean,m}], \tag{2}$$

I_r, expressed as unit less fraction, was calculated as the ratio of I_a (Equation (2)) and the seasonal sum of the monthly anomalies of the reference period as

$$I_r = \frac{\sum_{m=1}^{7} [\Delta_{2018,m} - \Delta_{mean,m}]}{\sum_{m=1}^{7} [\Delta_{mean,m}]}, \tag{3}$$

2.6. Statistical Methods

We provide a detailed analysis of ET, T_{sa}, and P changes across six contrasting regions in Europe by calculating descriptive statistics (i.e., mean, standard deviation) of monthly variables. The definition of the six different regions was based on contrasting drought characteristics in terms of onset, length, intensities, and the onset difference between ET and meteorological variables. The drought characteristics per region were classified into an ordinal scale. The ordinal scale was calculated by i) normalizing all drought characteristics between 0 to 1 and ii) replacing the value range with an ordinal scale according to the definition of each drought characteristic (Table 1). The normalization was based on the following equation:

$$N_{(a,b)} = \frac{[a - b]}{L}, \tag{4}$$

where $N_{(a,b)}$ is the normalized value between a (i.e., the maximum value of a drought characteristic of a specific region) and b (i.e., the minimum value of a drought characteristic of a specific region). L is the maximum value of a particular drought characteristic among all regions. Monthly anomalies of ET, T_{sa}, and P are extracted for each of the selected regions and stratified into six vegetation types, i.e., agriculture (AG), forest (FR), inland

marshes (IM), mixed natural vegetation (MNV), non-irrigated arable land (NIA), and peat bogs vegetation (PB).

Table 1. Relation of normalized value ranges and ordinal scale of drought characteristics.

| Normalized Value Range	Ordinal Scale of Drought Characteristics			
	Intensity	Onset	Length	Onset Difference
0.00 to 0.20	Low	Early emergence in April–May	Short $\leq$ 2 months	Early ET onset ~= −4 months
0.21 to 0.40	Medium	Emergence in May–June	Moderate ~= 3 months	Early ET onset ~= −2 months
0.41 to 0.60	Moderate	Emergence in June–July	Moderate ~= 4 months	Onset difference onset $\pm$ 1 month
0.61 to 0.80	High	Emergence in July–Aug	Moderate ~= 5 months	Late ET onset ~=2 months
0.81 to 1.00	Extreme	Late Emergence in Sept–Oct	Long $\geq$ 6 months	Late ET onset ~=4 months

3. Results

3.1. Characteristics of the Combined Heatwave and Drought in 2018

Monthly T_{sa} and P anomalies related to Europe's combined drought and heatwave in 2018 were used to characterize this extreme event in terms of onset, length, and absolute and relative intensities (Figure 2). Positive monthly T_{sa} anomalies appeared over central and eastern Europe in April, while the rest of the continent showed an onset of positive T_{sa} anomalies in May. The drought, expressed as negative P anomalies, started in early April in northern, central, and eastern Europe (Figure 2a). A notable exception is the Iberian Peninsula, with a much later arrival of the P anomaly between June to August (right of Figure 2a).

The T_{sa} duration mirrors the onset pattern with central and eastern Europe suffering up to seven months, and northern and western Europe up to six months (left of Figure 2b). The length of negative P anomalies was more diverse with longest durations (of up to seven months) in central Europe, moderate durations (four to five months) in South-East and North-West Europe as well as the southern part of Scandinavia, and short durations (one to three months) far North of Europe and south of the Alps. Exceptions are southern Europe with negative P anomalies lasting only up to three months and northern Europe with negative P and positive T_{sa} anomalies with lengths between one to three months (right of Figure 2b).

Seasonal anomalies (i.e., calculated as absolute and relative intensities compared to the reference period) were most severe in central Europe. This central region was affected most by increased T_{sa} (cumulated T_{sa} anomaly of up to 60 °C or 90% increase) and P deficits (up to −550 mm or −70%) for the seven months' time period per pixel (Figure 2c,d). The distribution of absolute T_{sa} intensities showed that particularly eastern and central Europe were affected with cumulated T_{sa} anomalies between 39 and 60 °C (Figure 2c) and relative cumulated T_{sa} intensities between 60% to more than 100% (Figure 2d). The heatwave was less pronounced in western Europe and over the Iberian Peninsula with cumulated T_{sa} anomalies ranging from 10 to 27 °C (Figure 2c) or 6% to 41% (Figure 2d). Pattern of the absolute P intensity showed substantial reductions of P in central Europe (−550 to −110 mm) and some parts of the Balkan Peninsula (−550 to −230 mm) (right of Figure 2c), corresponding to relative P intensities of −70% to −18% (right of Figure 2d). In contrast, substantially increased absolute P anomalies were observed in the far North of the Scandinavian Peninsula and some parts of southern Europe and South of the Alps (up to 600 mm or 23% to 80%) (right of Figure 2c,d).
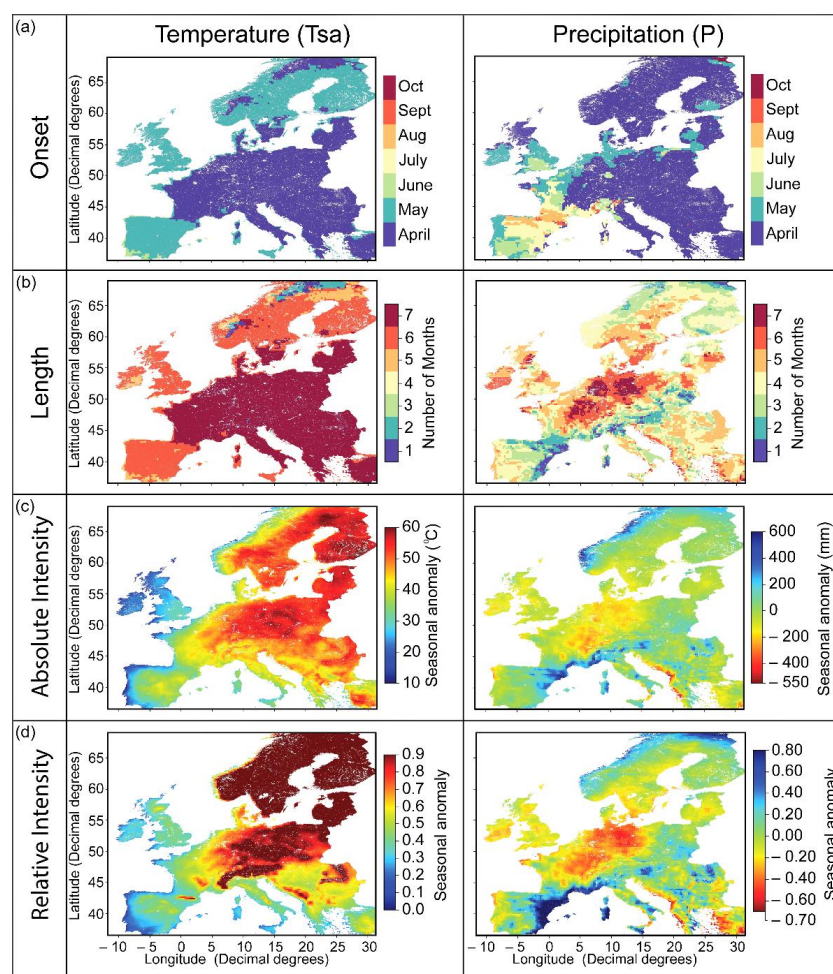
Figure 2. Characteristics of the Europe's combined drought and heatwave in 2018. (**a**) Onset, (**b**) length, (**c**) absolute intensity and (**d**) relative intensity of surface air temperature (T_{sa}) and precipitation (P) anomalies in 2018.

Overall, duration and intensity assessments of T_{sa} and P clearly illustrated a border between the dryer and wetter parts of Europe in 2018. The increased T_{sa} most affected eastern Europe along the full latitudinal gradient and particularly central Europe. Central Europe and the South of Scandinavia were additionally affected by a severe and prolonged drought (up to seven months), resulting in a substantial stress potential for ecosystems. The Iberian Peninsula and other regions South of the Alps showed contrasting pattern with low T_{sa} anomalies and more P compared to the reference period.

3.2. Spatio-Temporal Evaluation of Evapotranspiration Anomalies

A seasonal perspective on ET anomalies indicated significantly reduced ET fluxes, particularly in northern Europe, compared to southern Europe with a clear border along the Alps. Starting in April (Figure 3a), ET in most parts of Europe was close to its long-term baseline, with some areas in central and eastern Europe showing higher than normal ET, possibly linked to warm spring conditions (Figure 2). Few exceptions are visible in the North of the United Kingdom, in the South of the Balkan Peninsula, and in the part of the Iberian Peninsula with reduced ET (between −11% and −47%). In May (Figure 3b), negative ET anomalies in the South of the Balkan Peninsula became smaller, while negative ET anomalies now appeared in the North of the Iberian Peninsula and some areas in North-West Europe (−7 to −45% ET). Most areas in eastern and northern Europe and parts of the Iberian Peninsula showed positive ET anomalies (up to 66%).
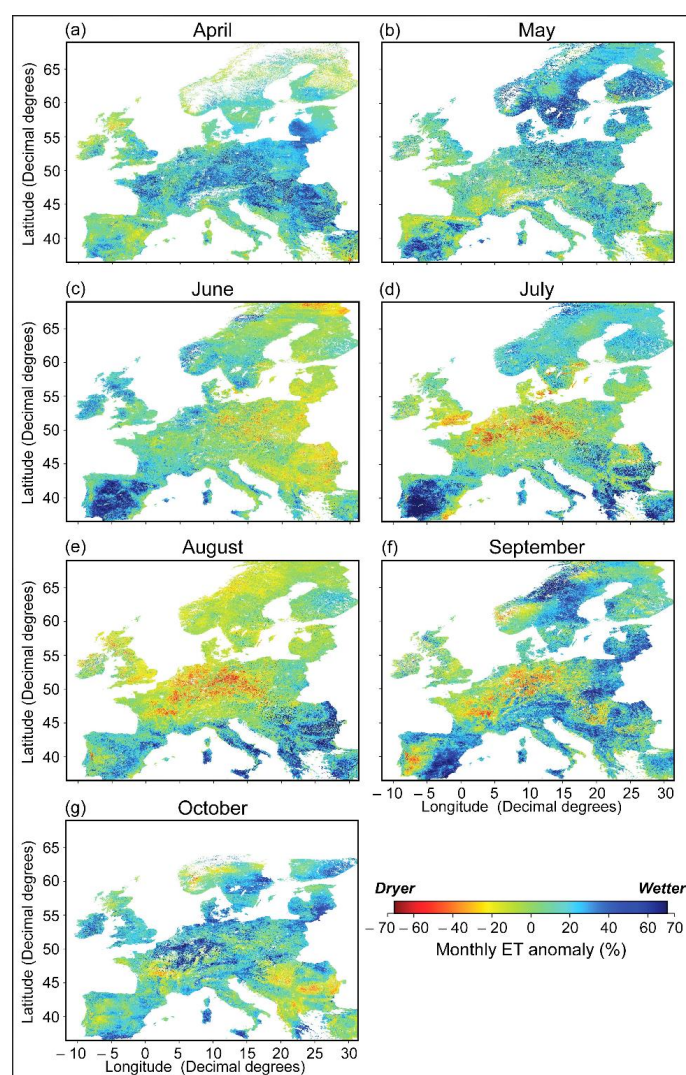
Figure 3. Evapotranspiration (ET) anomalies. Individual ET anomaly maps, from (**a**–**g**), show the normalized difference in percent between monthly mean ET for April to October 2018 (drought) compared to the reference monthly ET for April to October averaged between 2007 and 2017 (no drought). The maps are calculated from the MODerate Resolution Imaging Spectroradiometer (MODIS) MOD16A2 version 6 Total ET product. White-colored areas are either no-data or non-vegetation pixels.

June 2018 marked the onset of a substantial ET anomaly across central Europe. The development started in eastern Europe (Figure 3c), where ET anomalies became more negative over vast areas from North-East to South-East Europe (−1 to −62%). At the same time, West and North-West Europe developed a positive ET anomaly, while the Iberian Peninsula showed increased ET fluxes compared to the long-term reference of up to 70%. In July, the ET anomaly moved towards West and arrived over central Europe (Figure 3d). Central Europe showed reduced ET values between −1 and −70%. The South of Europe still had positive ET fluxes (up to +65 % over the Iberian Peninsula), while smaller but positive ET anomalies were observed in Scandinavia and over the Balkan Peninsula. In August (Figure 3e), substantial negative ET anomalies manifested in central Europe and approached northern and western Europe. In central Europe and North of the Alps, ET reduced down to −70%. In southern and South-East Europe, positive ET anomalies (up to 70%) were found.

In September, negative ET anomalies (from −3% to −70%) persisted over central and western Europe, in parts of Scandinavia, and developed in parts of the Iberian South-

West Peninsula (Figure 3f). The remaining parts of southern Europe and areas in the West of Europe developed a positive ET anomaly (up to 70%). In October (Figure 3g), the substantial negative ET anomaly slightly diminished from central Europe and appeared patchy across southern Europe with hot spots on the Balkan Peninsula −9% to −56%, parts of Scandinavia and South-West Europe (up to −59%).

3.3. Impact of Meteorological Driver Dynamics on Evapotranspiration Anomalies

We further analyzed observed ET anomaly patterns to unravel characteristics of the functional ecosystem response to T_{sa} and P dynamics. The early onset of negative ET anomalies (Figure 4a) started in southern Europe in April. Eastern Europe was affected by negative ET anomalies from May and June onwards. The results indicated a resilience of the ecosystems of 1–2 months compared to the onsets of T_{sa} and P anomalies (Figure 2a,b). Negative ET anomalies then moved towards western Europe in July and then northern Europe in August. The center of the Iberian Peninsula also showed a relatively late onset of a negative ET anomaly. Remarkably, the southern part of the Balkan Peninsula and the southwestern part of the Iberian Peninsula had the latest negative ET anomalies in October. The length of negative ET anomalies (Figure 4b) indicate that central Europe was longest affected (up to six months), while southern and northern Europe only short term (up to two months). An exception was a small area in the western part of the Iberian Peninsula, with the most extended negative ET anomaly (up to seven months).
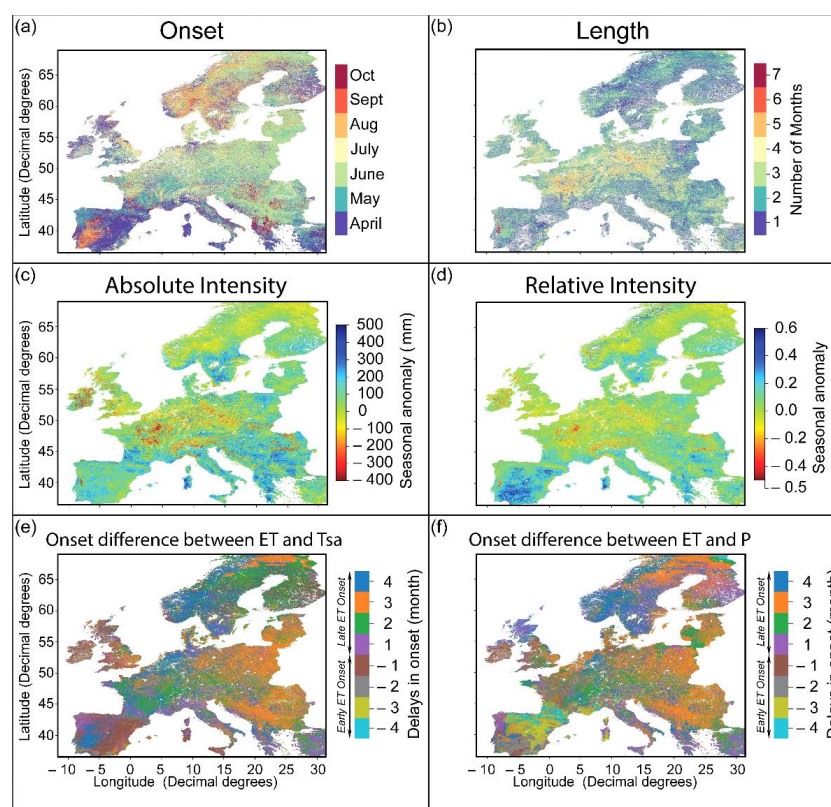
Figure 4. Characteristics of ecosystem response, represented as evapotranspiration (ET), to the extreme event. (**a**) Onset, (**b**) length, (**c**) absolute intensity, and (**d**) relative intensity of ET anomalies in 2018, and (**e**) difference between the onset of ET and surface air temperature (T_{sa}), and (**f**) difference between the onset of ET and precipitation (P).

Both absolute and relative intensities (Figure 4c,d) indicate most negative seasonal ET anomalies in central Europe (−400 mm or −50%). Northern Europe, the North of Scandinavia, eastern, and western Europe had moderate seasonal and patchy anomalies summing to values between −106 and 270 mm or −17 and 36%). Southern Europe,

particularly the Iberian and Balkan Peninsula, showed more positive seasonal ET anomalies (up to 500 mm or 60%) compared to other parts in Europe.

Since a delayed response in ET to environmental extremes is possible, we estimated the delays in the onset of ET compared to the onset of T_{sa} (Figure 4e) and P (Figure 4f). Compared to the onset of T_{sa}, ET onset delays increased from southwestern Europe (Iberian Peninsula) with delays between minus one to one month, to central Europe (two months) to eastern Europe (dominated by a delay of three months). The most prolonged delays of four months can be found in northern Europe, particularly Scandinavia, and in a small area of the Iberian Peninsula (Figure 4e). A similar spatio-temporal pattern can be found when comparing the onset of P and ET (Figure 4f). Exceptions are a more pronounced stratification with negative delays in the Iberian Peninsula and some areas in northern Europe that showed a longer delay (three to four months) between P and ET onset compared to the delay between T_{sa} and ET onset.

3.4. Ecosystem Specific ET Responses to the 2018 Drought

Detailed analysis of ET, T_{sa}, and P anomaly patterns and their characteristics indicated contrasting regions across Europe that were differently affected by the combined meteorological extreme event in 2018. An integrative visual representation of absolute intensities of T_{sa} and P (driver) and ET (ecosystem response) (Figure 5) was used to visualize the level of coherence between drought impact and ecosystem response. Based on this representation, six contrasting regions distributed across Europe were selected for further analysis. An overview of T_{sa}, P, and ET characteristics during the extreme event for the six selected regions is presented in Table 2.
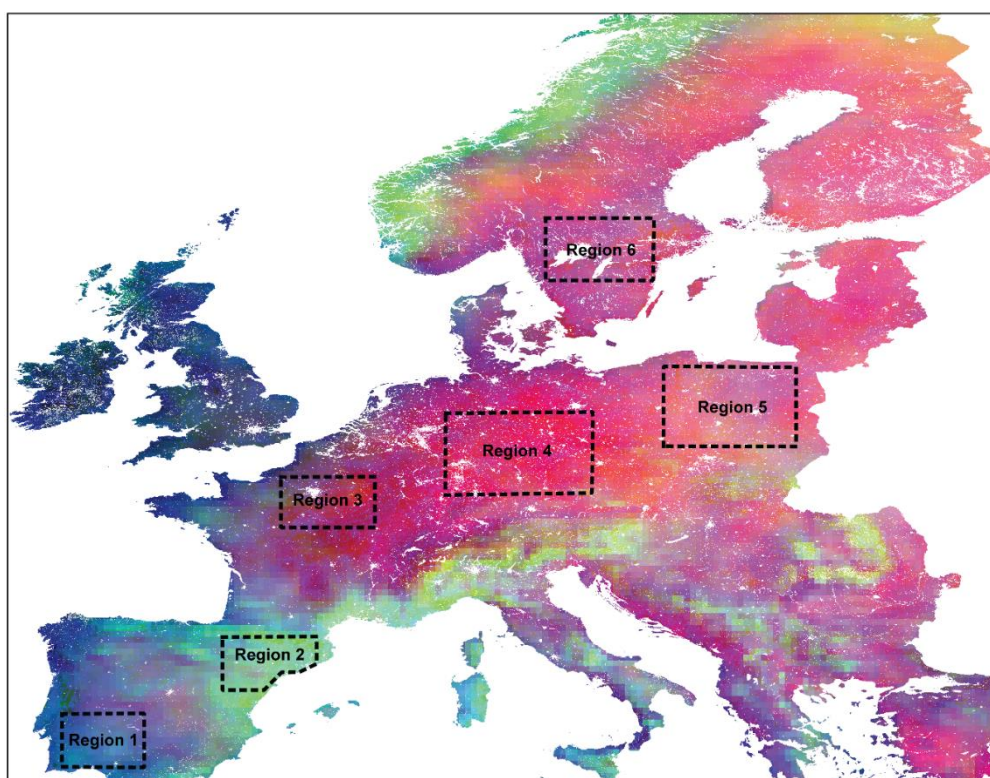
**Figure 5.** Comparative analysis of evapotranspiration (ET), surface air temperature (T_{sa}) and precipitation (P) anomaly pattern during the combined drought and heat wave in 2018. The black boundaries indicate contrasting regions of interest for further analysis. The base map is a false color composite, while Red-Green-Blue indicate absolute intensities of T_{sa}, ET, and P, respectively.

Table 2. Overview of drought characteristics for surface air temperature (T_{sa}), precipitation (P), and evapotranspiration (ET) for six selected regions distributed across Europe.

		Region1	Region2	Region3	Region4	Region5	Region6
Onset	T_{sa}						
	P						
	ET						
Length	T_{sa}						
	P						
	ET						
Intensity (Absolute)	T_{sa}						
	P						
	ET						
Intensity (Relative)	T_{sa}						
	P						
	ET						
Onset difference ET-T_{sa}							
Onset difference ET-P							

Ordinal scale for Onset, length, Intensity, and Onset difference			
Intensity	**Onset**	**Length**	**Onset difference**
Low	Early emergence in April–May	Short ≤ 2 months	Early ET onset ~= −4 months
Medium	Emergence in May–June	Moderate ~= 3 months	Early ET onset ~= −2 months
Moderate	Emergence in June–July	Moderate ~= 4 months	Onset difference onset ± 1 month
High	Emergence in July–Aug	Moderate ~= 5 months	Late ET onset ~= 2 months
Extreme	Late Emergence in Sept–Oct	Long ≥ 6 months	Late ET onset ~= 4 months

Region 1 is located in the Iberian Peninsula and represents a reference area with only a slight T_{sa} stress and a moderate P deficit (Figure 6a). The changes in monthly mean anomalies (Figure 6a) showed that, except for MNV and NIA, ET anomalies did not have negative values for all vegetation types from April to October, but rather positive values. MNV and NIA had negative ET anomalies only in September. Positive ET anomalies for all vegetation types increased from April (10% to 23%) to July (52% to 64%) and then decreased towards October (5% to 27%). An exception occurred in September for MNV and NIA vegetation types with a negative anomaly (MNV: −7%, NIA: −6%) and FR vegetation with a 0% anomaly. The monthly mean T_{sa} anomalies for region 1 showed a gradual increase from April (−9%) to August (56%) and then decreased until October (2%). The monthly P anomalies for region 1 showed the opposite of T_{sa} and ET anomalies with a gradual decrease from April (78%) to July (−79%) and a sharp increase until October (77%). Overall, ET anomalies for the six vegetation types and monthly mean T_{sa} anomalies had similar increasing and decreasing patterns. Comparing all anomalies, it becomes clear that region 1 was drier and warmer than the reference period (2007 to 2017) in terms of meteorological variables, but in terms of ET, region 1 was less affected by the extreme event.

Region 2 is located in southern Europe and is also a reference region with only a moderate T_{sa} stress and a low P deficit (Figure 6b). ET anomalies in this region were constantly above zero and increased for six vegetation types from April (2% to 14%) to June (17% to 50%). ET anomalies decreased in July (12% to 29%), then increased until September (30% to 34%) and decreased again in October (17% to 22%). An exception was NIA, with exceptionally higher ET values from May to August compared to other vegetation types. Monthly mean T_{sa} anomalies showed a gradual increase from April (−3%) to July (69%) and then a decrease until October (1%), while monthly mean P anomalies showed a decrease from April (80%) to July (−24%). The sharp decrease in the P anomaly in July was linked to a decrease of ET anomalies of about 20%. From July, P anomalies increased in August (5%), decreased in September (−9%) and sharply increased again in October (80%). Overall, region 2 was slightly dryer and warmer in 2018 compared to the reference period but wetter than region 1. ET was almost not affected by the extreme event, and even showed larger values compared to the reference period.
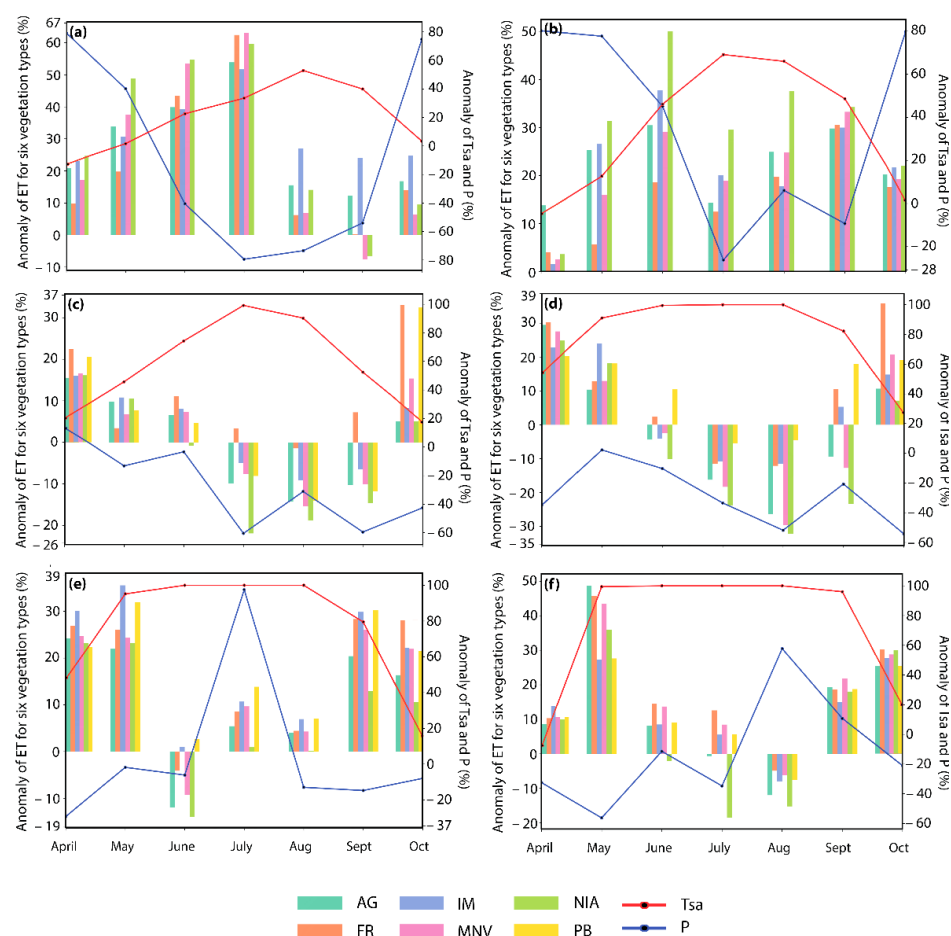
Figure 6. Changes in mean monthly ET anomalies (bar plots) for six different vegetation types [agriculture (AG), forest (FR), inland marshes (IM), mixed natural vegetation (MNV), and non-irrigated arable land (NIA), and peat bog vegetation (PB)], surface air temperature (T_{sa}) (red line), and precipitation (P) (blue line). Panels (**a–f**) represent regions 1–6. Both primary and secondary Y-axis are independently scaled for each region.

Region 3 is located in central-western Europe and represents one of the most drought-affected areas, while the heat-wave was less impacting compared to other regions further East (Figure 6c). ET anomalies for the six vegetation types showed a gradual decrease from April (17% to 23%) to July (−23% to 4%). From July until September ET anomalies were negative for most vegetation types and increased towards October (19% to 35%). An exception was FR, with slightly positive ET values in July and September. PB and FR showed exceptionally higher positive ET anomalies in October among the six vegetation types. The monthly mean T_{sa} anomalies for region 3 had no negative values but showed a seasonal behavior with low values in spring, high values in summer, and low values in autumn. The monthly mean T_{sa} anomaly gradually increased from April (21%) to July (99%) and then slightly decreased in August (95%). From August onwards, the anomaly decreased till October (19%). The monthly mean P anomaly decreased from April to October starting in April with a positive anomaly (17%) and then turned negative from May (−10%) to October (−41%) with largest reductions in July (−60%). Overall region 3 experienced a significant reduction in water inputs to ecosystems in 2018, which introduced considerable water shortage and impacted ecosystem ET.

Region 4 is located in central Europe and represents the hot spot of the drought and heatwave (Figure 6d). ET anomalies for six vegetation types in region 4 showed a decrease from April (21% to 30%) to August (−5% to −32%) and then increased until October (7% to 37%). Exceptions were FR and PB in June, and FR, IM, and PB in September

with positive values. Another exception was FR, with substantially higher positive ET values in October compared to the other vegetation types. The monthly mean T_{sa} anomaly showed no negative values, increased from April (56%) to May (95%) and then continued with highest values until August (99%). From August onwards, the monthly mean T_{sa} anomaly decreased till October (29%). Monthly mean P anomaly for region 4 were almost continuously negative ranging from 1% in May to −55% in October. Overall, neither T_{sa} nor P illustrated seasonal trends in changing anomalies. However, both meteorological variables showed severe dryness with continuous high T_{sa} and reduced P from May to September. The results indicate an extreme drought and heatwave, imposing a considerable reduction in ecosystem ET in 2018 compared to the reference period. The significant negative anomalies of P and ET, positive anomalies of T_{sa}, indicated that region 4 was driest among all regions.

Region 5 is located in eastern Europe and represents an area strongly affected by the heatwave and comparably less by P deficit (Figure 6e). ET anomalies for six vegetation types were lowest in June (2% to −17%), July (1% to 13%), and August (0% to 7%). Only in June, except for PB and IM, all vegetation types had negative ET anomalies. In all other months, ET showed no negative anomaly. The monthly mean T_{sa} anomaly showed no negative values but continuously high values from May (95%) to August (99%), identical to region 4. The T_{sa} anomaly was less severe in April (50%) and October (18%). The monthly mean P anomaly had considerable negative values from April (−34%) to October (−8%); one exception was July with exceptionally positive values (98%). T_{sa} and P showed a clear indication of overall raised heat into the environment and reduced water inputs in ecosystems. The results showed that during the 2018 summer, ecosystem ET of region 5 was affected by dryness and excessive heat with a peak ET reduction in summer.

Region 6 is located in the North of Europe on the Scandinavian Peninsula and represents, as region 5, another area affected by T_{sa} as dominating driver (Figure 6f). The ET anomalies for six different vegetation types increased from April (9% to 14%) to May (27% to 48%) and then decreased to June (−2% to 15%) until August (−15% to −5%). NIA was an exception in June with negative ET anomalies compared to other vegetation types. From September onwards, ET anomalies for all vegetation types were again positive reaching values between 22% to 29% in October. T_{sa} anomalies sharply increased from April (−8%) to May (98%), then stayed at very high values until September (96%) and dropped in October (21%). Monthly mean P anomalies showed more variation than T_{sa} anomalies. The anomalies started negative in April and May (−31% to −58%), then increased in June (−10%) and decreased in July (−34%). In August, the P anomaly sharply increased (58%) and dropped in towards October (−20%). Overall, ET was most reduced in summer (June to August), similar as in region 5. Both meteorological anomalies had significant negative and positive values, determining region 6 in 2018 as drier and warmer compared to the reference period.

4. Discussion

4.1. Considerations on Observed Drought Impact on Ecosystem Evapotranspiration

The combined drought and heatwave in 2018 had a substantial impact on the functioning of European ecosystems in general and on ET fluxes in particular. This finding agrees with recent studies, indicating that the drought in 2018 was even more severe than the drought that occurred in 2003 [43]. Our results showed that this combined climate event in 2018 emerged from northern and eastern Europe and continued to central and western Europe, and parts of southern Europe. Particularly the months of June to August 2018 were driest and hottest for most of central, northern, eastern, and western Europe, while climate reports also associated these months with anomalous weather conditions in most of the northern hemisphere, reaching in average 1.3 °C higher T_{sa} in northern and central Europe compared to a reference period [44] We also observed a very long (up to seven months) and severe drought mostly in central, eastern, northern, and western Europe in 2018 compared to the reference period (from 2007 to 2017), while the South and southern

Europe experienced a shorter and less severe drought (c.f. Figure 2b–d; Figure 4b–d). This is in agreement with a recent study stating that northern and central Europe, including the United Kingdom and Scandinavia, was the epicenter of the 2018 European drought, while southern Europe was colder and wetter in 2018 compared to the reference period [7]. This particular drought situation in 2018 can be related to a rare atmospheric synoptic situation, land-atmosphere interactions [45–47], prolonged warming trends [48], and the development and progression of the European drought along the season driven by large-scale mechanisms [49]. Due to the climatic dipole in 2018, southern Europe was less affected by the drought, even experienced the wettest spring and summer [43,50] and even a flooding in Spain and Greece [48].

Estimated ET anomalies showed large spatio-temporal variability across climatic regions and ecosystems, with ET substantially differing depending on climatic drivers (i.e., drought vs. non-drought conditions) and ecosystem types [3,4]. In central, northern, eastern, and western Europe, the ET onset emerged one to four months later than the combined heatwave and drought (c.f. Figure 4e,f). A previous study found that soil drought had a delayed effect on green water (water in the root zone) than on blue water (runoff) availability [15], and indicates that a reduction in ET occurred several months after the drought onset, while decreases in runoff happened shortly after the drought onset [15]. This is consistent with our finding that ET was reduced mostly in the summer months than in early 2018, due to the onset of the combined drought and the heatwave starting in April and May. In opposite, the onset of ET emerged one to four months earlier in the South-West and southern Europe than the onset of the drought and heatwave (c.f. Figure 4e,f), particularly in the Iberian Peninsula. This region is dominated by vegetation adapted to the Mediterranean's water-limited ecosystems and can better cope with drought than vegetation less adapted to droughts in northern Europe temperature-limited ecosystems [7,43]. However, the earlier onset of the ET anomaly is caused by an earlier drought that occurred in Italy in 2017 [51] and was not covered by our data series spanning only April to September 2018. In addition, ET intensities indicated that areas in northern Europe were more affected than southern Europe (Figures 2 and 4), which is coherent with the observed regional dipole pattern where the northern region of the Alps is warm and dry, and the southern regions are cold and wet [43]. Our results indicated that the intensity of ecosystem ET was mostly reduced in the areas with extreme intensities of T_{sa} and P anomalies in central, northern, eastern, and western Europe (i.e., ET was reduced up to 50%).

Concerning differences in regions and vegetation types, especially regions 3 in western Europe, 4 in central Europe, 5 in eastern Europe, and 6 in northern Europe were affected by extreme and long T_{sa} and P anomalies and showed a strong reduction in ET for all vegetation types between June and September. In opposite, regions 1 and 2 showed an increased ET for all vegetation types compared to the reference period. In the drought-affected regions (i.e., 3–6), particularly NIA, MNV, and AG showed larger reductions in ET (Figure 6). In fact, a recent study reported that pasture and arable lands were more sensitive than other ecosystems to the 2018 drought [43], and also grasslands, even at high elevation, were affected by the 2018 drought [6]. This is in agreement with our observation of large ET reductions in AG in many regions affected by the event. Furthermore, we found ET in MNV to be largely affected, which coincides with recent a study stating that forests in Austria, Germany, and Switzerland were severely affected by the 2018 European drought [5]. Our results show similar changes in monthly anomalies between ET together with T_{sa} and P for different regions. This indicates a close mechanistic interlink between ET as response variable [26] and T_{sa} and P as drivers [19,20,22–24]. Since other important abiotic drivers besides P and T_{sa} determine ET [26–28,52], the interpretation of such interrelations remains challenging but is essential for a sustainable and adaptive ecosystems management under climate change.

4.2. Reliability of this Study

Although our approach provides reliable and insightful information to assess ET dynamics under extreme climate events, we could only investigate potential rather than actual ET. In the absence of global observations directly connected to the process of photosynthesis at adequate spatial sampling distance (i.e., in the order of a few hundred meters), we used a quality product based on vegetation greenness indicative for potential ET. The severity of the drought impact enabled a reliable assessment, but subtle and early pre-visible drought responses cannot be investigated. The onset, length, and intensities of meteorological variables (Figure 2) illustrated characteristics of the drought and heatwave in 2018 and supported further analysis to interpret ET anomalies (Figure 3) across climate regions (Figure 4), and vegetation types (Figure 6).

Further, possible phenological shifts in ET and meteorological drivers during extreme events can impact the assessment and needs further considerations with longer time series and possibly better temporal resolution. It is also suggested to extend our analysis with additional context information to account for complex hydrological mechanisms specific for various catchments and ecosystems (e.g., topography [6]). Our analysis is limited in this sense and future research is required to reveal robust ecosystems specific interlink between ET and determinants of drought and heatwave (i.e., T_{sa} and P). Additional effects of used data might further compromise the representativeness of our results, i.e., inherently limited sensitivity to ecosystems specific processes due to the specific remote sensing perspective that only observes the outer canopy at a coarse spatial resolution [53].

5. Conclusions

From our results we conclude that the combined drought and heatwave in Europe in 2018 severely affected the functioning of ecosystems and caused substantial variations of related energy and water fluxes with a seasonally aggregated ET anomalies of up to −400 mm (or −50%) in central Europe. We observed correspondence of spatio-temporal intensity patterns between the extreme event and ET, but also found a time delay of one to four months between the occurrence of the extreme event and the onset of the ET anomaly, particularly in central, northern, eastern, and western Europe. This time delay coincided with a different duration of a negative ET anomalies (three to seven months) compared to the duration of the extreme event.

The severity of the investigated drought allowed assessing related ET dynamics with common observational approaches sensitive for potential rather than actual ET. We suggest implementing approaches that allow assessing actual ET rates and partitioning ET into the component fluxes of transpiration and evaporation for further precise assessment of the impact of drought on ET. Such strategies will allow to investigate more sudden ecosystem responses to environmental stress and to disentangle varying interwoven processes that were bulky assessed in this study, and thus advance understanding on complex climate-ecosystem feedbacks on ET.

Author Contributions: K.R.A. designed the research with scientific advice by E.P.-L. and A.D.; data analysis done by K.R.A. and A.D.; evaluation of results by K.R.A., E.P.-L., U.R. and A.D.; data visualization by K.R.A.; K.R.A. wrote the manuscript and all co-authors thoroughly reviewed and edited the text. All authors have read and agreed to the published version of the manuscript.

Conflicts of Interest: The authors declare no conflict of interest.

References

1. Reichstein, M.; Bahn, M.; Ciais, P.; Frank, D.; Mahecha, M.D.; Seneviratne, S.I.; Zscheischler, J.; Beer, C.; Buchmann, N.; Frank, D.C.; et al. Climate Extremes and the Carbon Cycle. *Nature* **2013**, *500*, 287–295. [CrossRef]

2. Sippel, S.; Reichstein, M.; Ma, X.; Mahecha, M.D.; Lange, H.; Flach, M.; Frank, D. Drought, Heat, and the Carbon Cycle: A Review. *Curr. Clim. Chang. Rep.* **2018**, *4*, 266–286. [CrossRef]

3. Bonan, G.B. Forests and Climate Change: Forcings, Feedbacks, and the Climate Benefits of Forests. *Science* **2008**, *320*, 1444–1449. [CrossRef]

4. Anderegg, W.R.L.; Berry, J.A.; Smith, D.D.; Sperry, J.S.; Anderegg, L.D.L.; Field, C.B. The Roles of Hydraulic and Carbon Stress in a Widespread Climate-Induced Forest Die-Off. *Proc. Natl. Acad. Sci. USA* **2012**, *109*, 233–237. [CrossRef]

5. Schuldt, B.; Buras, A.; Arend, M.; Vitasse, Y.; Beierkuhnlein, C.; Damm, A.; Gharun, M.; Grams, T.E.E.; Hauck, M.; Hajek, P.; et al. A First Assessment of the Impact of the Extreme 2018 Summer Drought on Central European Forests. *Basic Appl. Ecol.* **2020**, *45*, 86–103. [CrossRef]

6. Gharun, M.; Hörtnagl, L.; Paul-Limoges, E.; Ghiasi, S.; Feigenwinter, I.; Burri, S.; Marquardt, K.; Etzold, S.; Zweifel, R.; Eugster, W.; et al. Physiological Response of Swiss Ecosystems to 2018 Drought across Plant Types and Elevation. *Philos. Trans. R. Soc. B Biol. Sci.* **2020**, *375*. [CrossRef]

7. Peters, W.; Bastos, A.; Ciais, P.; Vermeulen, A. A Historical, Geographical and Ecological Perspective on the 2018 European Summer Drought. *Philos. Trans. R. Soc. B* **2020**, *375*, 8. [CrossRef] [PubMed]

8. Lawrence, D.M.; Thornton, P.E.; Oleson, K.W.; Bonan, G.B. The Partitioning of Evapotranspiration into Transpiration, Soil Evaporation, and Canopy Evaporation in a GCM: Impacts on Land–Atmosphere Interaction. *J. Hydrometeorol.* **2007**, *8*, 862–880. [CrossRef]

9. Lu, X.; Liu, Z.; An, S.; Miralles, D.G.; Maes, W.; Liu, Y.; Tang, J. Potential of Solar-Induced Chlorophyll Fluorescence to Estimate Transpiration in a Temperate Forest. *Agric. For. Meteorol.* **2018**, *252*, 75–87. [CrossRef]

10. Zhang, Y.; Peña-Arancibia, J.L.; McVicar, T.R.; Chiew, F.H.S.; Vaze, J.; Liu, C.; Lu, X.; Zheng, H.; Wang, Y.; Liu, Y.Y.; et al. Multi-Decadal Trends in Global Terrestrial Evapotranspiration and Its Components. *Sci. Rep.* **2016**, *6*, 19124. [CrossRef] [PubMed]

11. Ge, Z.-M.; Kellomäki, S.; Zhou, X.; Wang, K.-Y.; Peltola, H.; Väisänen, H.; Strandman, H. Effects of Climate Change on Evapotranspiration and Soil Water Availability in Norway Spruce Forests in Southern Finland: An Ecosystem Model Based Approach: STAND HYDRO-PROCESSES UNDER CLIMATE CHANGE. *Ecohydrology* **2013**, *6*, 51–63. [CrossRef]

12. Anderegg, W.R.L.; Kane, J.M.; Anderegg, L.D.L. Consequences of Widespread Tree Mortality Triggered by Drought and Temperature Stress. *Nat. Clim. Chang.* **2013**, *3*, 30–36. [CrossRef]

13. Bennett, A.C.; McDowell, N.G.; Allen, C.D.; Anderson-Teixeira, K.J. Larger Trees Suffer Most during Drought in Forests Worldwide. *Nat. Plants* **2015**, *1*, 15139. [CrossRef]

14. Gu, D.; Wang, Q.; Otieno, D. Canopy Transpiration and Stomatal Responses to Prolonged Drought by a Dominant Desert Species in Central Asia. *Water* **2017**, *9*, 404. [CrossRef]

15. Orth, R.; Destouni, G. Drought Reduces Blue-Water Fluxes More Strongly than Green-Water Fluxes in Europe. *Nat. Commun.* **2018**, *9*, 3602. [CrossRef]

16. Leuning, R.; Zhang, Y.Q.; Rajaud, A.; Cleugh, H.; Tu, K. A Simple Surface Conductance Model to Estimate Regional Evaporation Using MODIS Leaf Area Index and the Penman-Monteith Equation: MODIS-LAI-BASED EVAPORATION MODEL. *Water Resour. Res.* **2008**, *44*. [CrossRef]

17. Vetter, M.; Churkina, G.; Jung, M.; Reichstein, M.; Zaehle, S.; Bondeau, A.; Chen, Y.; Ciais, P.; Feser, F.; Freibauer, A.; et al. Analyzing the Causes and Spatial Pattern of the European 2003 Carbon Flux Anomaly Using Seven Models. *Biogeosciences* **2008**, *5*, 561–583. [CrossRef]

18. Gao, Y.; Markkanen, T.; Aurela, M.; Mammarella, I.; Thum, T.; Tsuruta, A.; Yang, H.; Aalto, T. Response of Water Use Efficiency to Summer Drought in a Boreal Scots Pine Forest in Finland. *Biogeosciences* **2017**, *14*, 4409–4422. [CrossRef]

19. Baltas, E. Spatial Distribution of Climatic Indices in Northern Greece. *Meteorol. Appl.* **2007**, *14*, 69–78. [CrossRef]

20. Vicente-Serrano, S.M.; Beguería, S.; López-Moreno, J.I. A Multiscalar Drought Index Sensitive to Global Warming: The Standardized Precipitation Evapotranspiration Index. *J. Clim.* **2010**, *23*, 1696–1718. [CrossRef]

21. Anderson, M.C.; Hain, C.; Wardlow, B.; Pimstein, A.; Mecikalski, J.R.; Kustas, W.P. Evaluation of Drought Indices Based on Thermal Remote Sensing of Evapotranspiration over the Continental United States. *J. Clim.* **2011**, *24*, 2025–2044. [CrossRef]

22. Guttman, N.B. COMPARING THE PALMER DROUGHT INDEX AND THE STANDARDIZED PRECIPITATION INDEX. *J. Am. Water Resour. Assoc.* **1998**, *34*, 113–121. [CrossRef]

23. Tian, L.; Leasor, Z.T.; Quiring, S.M. Developing a Hybrid Drought Index: Precipitation Evapotranspiration Difference Condition Index. *Clim. Risk Manag.* **2020**, *29*, 100238. [CrossRef]

24. Kim, D.; Rhee, J. A Drought Index Based on Actual Evapotranspiration from the Bouchet Hypothesis: DROUGHT INDEX FROM BOUCHET HYPOTHESIS. *Geophys. Res. Lett.* **2016**, *43*, 10277–10285. [CrossRef]

25. Keyantash, J.A.; Dracup, J.A. An Aggregate Drought Index: Assessing Drought Severity Based on Fluctuations in the Hydrologic Cycle and Surface Water Storage: AN AGGREGATE DROUGHT INDEX. *Water Resour. Res.* **2004**, *40*. [CrossRef]

26. Allen, R. PENMAN–MONTEITH EQUATION. In *Encyclopedia of Soils in the Environment*; Elsevier: Amsterdam, The Netherlands, 2005; pp. 180–188.

27. Fisher, J.B.; Melton, F.; Middleton, E.; Hain, C.; Anderson, M.; Allen, R.; McCabe, M.F.; Hook, S.; Baldocchi, D.; Townsend, P.A.; et al. The Future of Evapotranspiration: Global Requirements for Ecosystem Functioning, Carbon and Climate Feedbacks, Agricultural Management, and Water Resources: THE FUTURE OF EVAPOTRANSPIRATION. *Water Resour. Res.* **2017**, *53*, 2618–2626. [CrossRef]

28. Pereira, L.S.; Perrier, A.; Allen, R.G.; Alves, I. Evapotranspiration: Concepts and Future Trends. *J. Irrig. Drain. Eng.* **1999**, *125*, 45–51. [CrossRef]

29. Van Loon, A.F. Hydrological Drought Explained: Hydrological Drought Explained. *Wiley Interdiscip. Rev. Water* **2015**, *2*, 359–392. [CrossRef]

30. Destouni, G.; Verrot, L. Screening Long-Term Variability and Change of Soil Moisture in a Changing Climate. *J. Hydrol.* **2014**, *516*, 131–139. [CrossRef]

31. Naumann, G.; Spinoni, J.; Vogt, J.V.; Barbosa, P. Assessment of Drought Damages and Their Uncertainties in Europe. *Env. Res Lett* **2015**, *10*, 124013. [CrossRef]

32. Gudmundsson, L.; Rego, F.C.; Rocha, M.; Seneviratne, S.I. Predicting above Normal Wildfire Activity in Southern Europe as a Function of Meteorological Drought. *Environ. Res. Lett.* **2014**, *9*, 084008. [CrossRef]

33. Mu, Q.; Heinsch, F.A.; Zhao, M.; Running, S.W. Development of a Global Evapotranspiration Algorithm Based on MODIS and Global Meteorology Data. *Remote Sens. Environ.* **2007**, *111*, 519–536. [CrossRef]

34. Mu, Q.; Zhao, M.; Running, S.W. Improvements to a MODIS Global Terrestrial Evapotranspiration Algorithm. *Remote Sens. Environ.* **2011**, *115*, 1781–1800. [CrossRef]

35. Penman, H.L. Natural Evaporation from Open Water, Bare Soil and Grass. *Proc. R. Soc. Lond. Ser. Math. Phys. Sci.* **1948**, *193*, 120–145.

36. Monteith, J.L.; Szeicz, G.; Waggoner, P.E. The Measurement and Control of Stomatal Resistance in the Field. *J. Appl. Ecol.* **1965**, *2*, 345. [CrossRef]

37. Gorelick, N.; Hancher, M.; Dixon, M.; Ilyushchenko, S.; Thau, D.; Moore, R. Google Earth Engine: Planetary-Scale Geospatial Analysis for Everyone. *Remote Sens. Environ.* **2017**, *202*, 18–27. [CrossRef]

38. Pérez, F.; Granger, B.E. IPython A System for Interactive Scientific Computing. *Comput. Sci. Eng.* **2007**, *9*, 21–29.

39. Virtanen, P.; Gommers, R.; Oliphant, T.E.; Haberland, M.; Reddy, T.; Cournapeau, D.; Burovski, E.; Peterson, P.; Weckesser, W.; Bright, J.; et al. SciPy 1.0–Fundamental Algorithms for Scientific Computing in Python. *Nat. Methods* **2020**, *17*, 261–272. [CrossRef]

40. van der Walt, S.; Colbert, S.C.; Varoquaux, G. The NumPy Array: A Structure for Efficient Numerical Computation. *Comput. Sci. Eng.* **2011**, *13*, 22–30. [CrossRef]

41. McKinney, W. Data Structures for Statistical Computing in Python. In Proceedings of the 9th Python in Science Conference (SciPy 2010), Austin, TX, USA, 28 June–3 July 2010; pp. 56–61.

42. Hunter, J.D. Matplotlib: A 2D Graphics Environment. *Comput. Sci. Eng.* **2007**, *9*, 90–95. [CrossRef]

43. Buras, A.; Rammig, A.; Zang, C.S. Quantifying Impacts of the 2018 Drought on European Ecosystems in Comparison to 2003. *Biogeosciences* **2020**, *17*, 1655–1672. [CrossRef]

44. NOAA. *National Centers for Environmental Information, State of the Climate: Global Climate Report for July 2018*; National Oceanic and Atmospheric Administration, 2018; Published online August 2018. Available online: https://www.ncdc.noaa.gov/sotc/global/201807 (accessed on 29 November 2020).

45. Miralles, D.G.; Teuling, A.J.; van Heerwaarden, C.C.; Vilà-Guerau de Arellano, J. Mega-Heatwave Temperatures Due to Combined Soil Desiccation and Atmospheric Heat Accumulation. *Nat. Geosci.* **2014**, *7*, 345–349. [CrossRef]

46. Luterbacher, J.; Liniger, M.A.; Menzel, A.; Estrella, N.; Della-Marta, P.M.; Pfister, C.; Rutishauser, T.; Xoplaki, E. Exceptional European Warmth of Autumn 2006 and Winter 2007: Historical Context, the Underlying Dynamics, and Its Phenological Impacts. *Geophys. Res. Lett.* **2007**, *34*, 1–6. [CrossRef]

47. Mueller, B.; Seneviratne, S.I. Hot Days Induced by Precipitation Deficits at the Global Scale. *Proc. Natl. Acad. Sci. USA* **2012**, *109*, 12398–12403. [CrossRef] [PubMed]

48. Drouard, M.; Kornhuber, K.; Woollings, T. Disentangling Dynamic Contributions to Summer 2018 Anomalous Weather Over Europe. *Geophys. Res. Lett.* **2019**, *46*, 12537–12546. [CrossRef]

49. Quesada, B. Asymmetric European Summer Heat Predictability from Wet and Dry Southern Winters and Springs. *Nat. Clim. Chang.* **2012**, *2*, 6. [CrossRef]

50. C3S. *European State of the Climate 2018; Compiled by the Copernicus Climate Change Service (C3S), Implemented by the European Centre for Medium-Range Weather Forecasts (ECMWF) on Behalf of the European Union*; European Union, 2019. Published online September 2018. Available online: https://climate.copernicus.eu/ESOTC/2018 (accessed on 29 November 2020).

51. Puletti, N.; Mattioli, W.; Bussotti, F.; Pollastrini, M. Monitoring the Effects of Extreme Drought Events on Forest Health by Sentinel-2 Imagery. *J. Appl. Remote Sens.* **2019**, *13*, 1. [CrossRef]

52. Allen, R.G.; Tasumi, M.; Trezza, R. Satellite-Based Energy Balance for Mapping Evapotranspiration with Internalized Calibration (METRIC)—Model. *J. Irrig. Drain. Eng.* **2007**, *133*, 380–394. [CrossRef]

53. Damm, A.; Paul-Limoges, E.; Kükenbrink, D.; Bachofen, C.; Morsdorf, F. Remote Sensing of Forest Gas Exchange: Considerations Derived from a Tomographic Perspective. *Glob. Chang. Biol.* **2020**, *26*, 2717–2727. [CrossRef]